Effects of Martian conditions on numerically modeled, cooling-limited, channelized lava flows

Scott K. Rowland

Hawai'i Institute of Geophysics and Planetology, School of Ocean and Earth Science and Technology, University of Hawai'i at Mānoa, Honolulu, Hawai'i, USA

Andrew J. L. Harris

Hawai'i Institute of Geophysics and Planetology, and Department of Geology and Geophysics, School of Ocean and Earth Science and Technology, University of Hawai'i at Mānoa, Honolulu, Hawai'i, USA

Harold Garbeil

Hawai'i Institute of Geophysics and Planetology, School of Ocean and Earth Science and Technology, University of Hawai'i at Mānoa, Honolulu, Hawai'i, USA

[1]   We used the FLOWGO thermorheological model to examine the effects of Martian gravitational and environmental conditions on the cooling-limited behavior of lava flowing in a channel. The largest effect is due to the lower gravity on Mars as compared to Earth, which causes lava to flow more slowly. The lower velocity means that heat loss per distance down a Mars channel is greater even though the lower velocity also produces a higher percentage cover of insulating crust. Gravity alone causes the Mars flow to be >65 km shorter than an Earth flow with an equivalent volumetric flow rate. The cooler ambient Mars atmosphere causes a slight increase in heat loss by forced convection. This slows the flow a bit more, resulting in a very slight increase in heat loss per distance by all mechanisms, and decreases the modeled flow length by ∼1 km, a difference well below our model uncertainty. Replacing terrestrial values of atmospheric density, viscosity, thermal conductivity, heat capacity, and cubic expansivity makes convection less efficient and increases flow length by ∼15 km. Nevertheless, at the same volumetric flow rate, lava flows ∼50 km less far under Martian conditions than under terrestrial conditions. Our specific model flow has a volumetric flow rate of ∼5000 m^3 s^{-1} and traveled ∼190 km down a channel on a constant 7° slope. This volumetric flow rate is slightly less than the maximum rates during the 1783–1785 Laki eruption and is 5–10 times greater than those of typical Mauna Loa eruptions.   *INDEX TERMS:* 8429 Volcanology: Lava rheology and morphology; 8450 Volcanology: Planetary volcanism (5480); 8414 Volcanology: Eruption mechanisms; 8499 Volcanology: General or miscellaneous; *KEYWORDS:* cooling-limited, lava flows, Mars

1.   Introduction

[2]   Two main strategies have been used previously in attempts to model emplacement of lava flows. The first applies the results from *Hulme* [1974] showing that the planimetric shape and cross-flow profile of a lava flow are determined by the rheological properties of the lava at the time it was emplaced. Parameters such as channel morphology, flow width, thickness, and length can all be related to lava viscosity and yield strength if certain assumptions are made about the lava rheology. Examples include the use of channel dimensions to determine lava yield strengths [*Hulme*, 1974; *Fink and Zimbelman*, 1986, 1990; *Wadge and Lopes*, 1991]. Once the rheological properties of the

lavas are known or estimated (which can introduce considerable uncertainty), the underlying slopes and dimensions of channels and lobes can be used to determine flow velocities, most often utilizing the Jeffrey's formula [e.g., *Jeffreys*, 1925; *Johnson*, 1970; *Fink and Zimbelman*, 1990]:

$$V_c = \rho_{lava} \; g \; \sin \theta \; d^2 (n \; \eta_{lava})^{-1} \quad \text{or} \quad V_l = \rho_{lava} \; g \; h^2 (3 \; \eta_{lava})^{-1}. \tag{1}$$

Here, V_c is the velocity in a channel and n is a shape term that depends on the ratio between channel depth (d) and width [*Wadge and Lopes*, 1991] (a list of variables and constants is presented in Table 1). Other terms are lava density (ρ_{lava}), gravity (g), the underlying slope (θ), and the dynamic viscosity of the lava (η_{lava}). The second formulation is for nonchannelized flow lobes, with V_l as the lobe

Table 1. Variables and Constants

Symbol	Name	Value	Equation	Comments
$\mathcal{A}$	constant for calculating α_{atmos}	-0.01183 W m^{-1} K^{-1}	A6	
a	constant for calculating C_{atmos}	44.2 J K^{-1} mol^{-1}	A7	
a	constant for calculating η_{atmos}	533° Rankine	A5	
α_{atmos}	thermal conductivity of atmosphere	variable down flow	8, A6	*Kays and Crawford* [1980] for Earth, or calculated down flow for Mars
α_{lava}	thermal conductivity of lava	variable down flow		
$\mathcal{B}$	constant for calculating α_{atmos}	1.0174×10^{-4} W m^{-1} K^{-2}	A6	
b	constant for calculating C_{atmos}	8.8×10^{-3} J K^{-2} mol^{-1}	A7	
b	term for calculating η_{atmos}	calculated down flow	A5	Requires temporary conversion from C° to Rankine°
β_{atmos}	atmospheric thermal diffusivity	T_{atmos}^{-1}	8	
$\mathcal{C}$	constant for calculating α_{atmos}	-2.2242×10^{-8} W m^{-1} K^{-3}	A6	
c	constant for calculating C_{atmos}	-8.6×10^{5} J K mol^{-1}	A7	
C_{atmos}	molar heat capacity	variable down flow	A7	*Kays and Crawford* [1980] for Earth, or calculated down flow for Mars
C_H	wind friction factor	0.0036	3	*Greeley and Iverson* [1987]; *Keszthelyi and Denlinger* [1996]
cp$_{atmos}$	atmospheric specific heat capacity	variable down flow	3, A7	*Kays and Crawford* [1980] for Earth, or calculated down flow for Mars
d	channel depth	defined at vent	1, 2	Held constant down flow
ε	emissivity of basalt	0.95	4	
E_r	volumetric flow rate	constant	7	Determined from at-vent channel dimensions and velocity
f_{crust}	percent crust on channel surface	dependent on surface velocity, calculated down flow	4	
g	gravitational acceleration	9.8 m s^{-2} (Earth), 3.7 m s^{-2} (Mars)	1, 2	
η_{lava}	dynamic viscosity of lava	1000 Pa s at vent, recalculated down flow	1, 2, 6	*Dragoni* [1989]; *Pinkerton and Stevenson* [1992]
η_{atmos}	dynamic viscosity of atmosphere	variable down flow	8, A5	*Kays and Crawford* [1980] for Earth, or calculated down flow for Mars
H_b	thickness of basal crust	10% of channel depth	5	
h	lobe thickness	calculated down flow	1	
θ	underlying slope	7°	1, 2	held constant for this study
κ_{atmos}	atmospheric cubic expansivity	calculated down flow	A8	
L_{cryst}	latent heat of crystallization	3.5×10^{5} J kg^{-1}	7	
n	channel shape constant	2 (d ≪ w), 4 (d ≈ w)	1	depends on channel cross-section shape
ω	constant for calculating viscosity	0.04 K^{-1}		*Dragoni* [1989]
P_{Mars}	Mars atmospheric pressure	600 Pa	A1	*Hess et al.* [1977]; *Ryan et al.* [1978]
Q_{cond}	conductive heat loss	calculated down flow	5	
Q_{cryst}	crystallization heat gain	calculated down flow	7	
Q_{force}	forced convection heat loss	calculated down flow	3	FLOWGO uses the greater of Q_{force} or Q_{free} [*Head and Wilson*, 1986]
Q_{free}	free convection heat loss	calculated down flow	8	FLOWGO uses the greater of Q_{force} or Q_{free} [*Head and Wilson*, 1986]
Q_{rad}	radiative heat loss	calculated down flow	4	
Q_{visc}	viscous dissipation heat gain	calculated down flow	6	
ρ_{lava}	lava density	2600 kg m^{-3}	1, 2	1984 Mauna Loa basalt value
ρ_{atmos}	atmospheric density	variable down flow	8, A1	*Kays and Crawford* [1980] for Earth, or calculated down flow for Mars
R_{Mars}	ideal gas constant	0.19 J mol^{-1} K^{-1}	A1	M. Smith (personal communication, 2003)
$\mathcal{S}$	Sutherland's constant	240 °Rankine		Used for calculating a and b, and in turn η_{atmos}
σ	Stefan-Boltzmann constant	5.67×10^{-8} W m^{-2} K^{-4}	4	
$T_{ambient}$	ambient atmospheric temperature	20°C (Earth), -63°C (Mars)	A2	Mars temperature from *Hess et al.* [1977]; *Ryan et al.* [1978]

Table 1. (continued)

Symbol	Name	Value	Equation	Comments
T_{atmos}	average of ambient atmospheric and effective lava surface temperatures	calculated down flow	8, A1	
T_{core}	temperature of flow core	calculated down flow	7	
T_{crust}	temperature of cool surface component	calculated down flow	4	
T_{erupt}	flow core temperature at vent	1140°C		1984 Mauna Loa lava; *Lipman and Banks* [1987]
T_e	effective lava surface temperature	calculated down flow	A2, A3	
T_{hot}	temperature of hot surface component	calculated down flow	4	
T_0	reference temperature for CO_2	528° Rankine	A5	*Lide* [2001]
ΔT_{base}	temperature difference between lava and substrate	700°C (Earth, small-Earth)	5	Treated as a constant for lava flowing in an established channel
ΔT_{surf}	temperature difference between T_e and $T_{ambient}$	calculated down flow	3	
$\tau_{base-of-core}$	shear stress at base of flow core	calculated down flow	2	*Dragoni* [1989]; *Pinkerton and Stevenson* [1992]; *Rowland et al.* [2004]
U	wind speed	5 m s^{-1}	3	*Hess et al.* [1977]; *Ryan et al.* [1978]
υ_{atmos}	kinematic viscosity of atmosphere	variable down flow	8	*Kays and Crawford* [1980] for Earth, or calculated down flow for Mars
V_c	mean channel velocity	calculated down flow	1, 2	
V_l	lobe velocity	included for comparison	1	
φ_{cryst}	volume% crystals	variable down flow	7	*Kays and Crawford* [1980] for Earth, or calculated down flow for Mars
YS_{core}	yield strength of flow core	calculated down flow	2	*Dragoni* [1989]; *Pinkerton and Stevenson* [1992]

velocity and h as the lobe thickness. More complex pressure-driven and gravity+pressure-driven equations have also been developed, both for infinite sheets and for channels [e.g., *Sakimoto et al.*, 1997; *Sakimoto and Gregg*, 2001]; however, these also require input values of rheological properties. Additionally, they become nearly intractable if rheology is allowed to vary downslope. Moreover, it has been noted (S. Baloga, personal communication, 2003) that increasingly complex flow formulations produce negligible differences in calculated flow rates.

[3] The second major strategy for determining eruption parameters has been to study the thermal properties of flowing lava [e.g., *Baloga and Pieri*, 1986; *Dragoni*, 1989; *Crisp and Baloga*, 1990, 1994; *Harris et al.*, 1998]. These techniques are based on calculating the processes of heat loss and gain that occur as lava advances downslope. The problem is essentially to determine (for a given lava-flow or lava-channel dimension) the volumetric flow rate that lava must possess so that it does not solidify before reaching a particular distance from the vent. Refinement of both the lava-morphology and thermal-budget techniques has produced evermore complicated mathematical expressions that take into account more and more details of flow processes and lava properties [e.g., *Crisp and Baloga*, 1994; *Keszthelyi*, 1995a; *Harris and Rowland*, 2001].

2. FLOWGO Thermorheological Model

[4] FLOWGO [*Harris and Rowland*, 2001] (Figure 1) is a thermorheological model that tracks the heat gains and losses of an element of lava flowing down a partially user-defined channel. While doing so, FLOWGO recalculates all heat-dependent terms that affect the flow of this particular element and uses these to determine how fast it advances each increment down the channel. As such, the model is self-adaptive and able to interrelate all the processes that take place as lava cools and flows. FLOWGO was tested for its ability to replicate the final dimensions of the 1984 Mauna Loa flow as well as a 1997 Kīlauea flow and a 1998 Etna flow. End-member models were presented and these were based on maximizing (hot model) and minimizing (cold model) heat-loss controls such as starting crystallinity and crust temperatures. The hot and cold model results bracketed the actual channel lengths in the test flows. *Harris and Rowland* [2001] noted that additional spread in
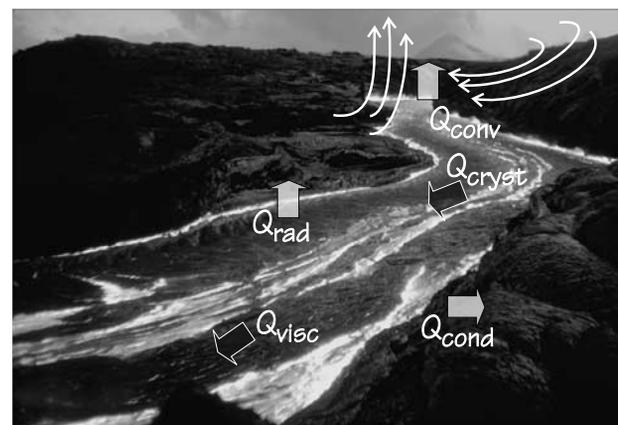

Figure 1. Schematic diagram showing the heat loss and gain terms calculated by FLOWGO for lava flowing in an open channel on Mars.

the results occurs because of uncertainties about input starting rheological properties (viscosity, yield strength, vesicularity, etc.).

[5] FLOWGO models cooling-limited flows [e.g., *Guest et al.*, 1987; *Pinkerton and Wilson*, 1994], meaning that lava stops when heat losses raise viscosity and/or yield strength to the point that deformation can no longer occur. The alternative, not modeled by FLOWGO, is supply-limited behavior where insulated flows (i.e., in lava tubes) stop only when the supply at the vent ceases [e.g., *Guest et al.*, 1987; *Pinkerton and Wilson*, 1994].

[6] The heat-losses that FLOWGO assesses are those due to radiation, convection (the greater of forced or free), conduction, and vaporization of rainwater. Heat gains are due to latent heat of crystallization and viscous dissipation. The following summarizes modeled results for tholeiite basalt input parameters and subaerial emplacement. Heat loss is dominated by radiation, which except at the lowest temperatures outweighs by at least an order of magnitude the combined heat losses from convection and conduction. Typical maximum rainfall rates on the windward slopes of Mauna Loa are 10^{-3} mm s^{-1} [e.g., *Mordy*, 1957] and this has a negligible effect on FLOWGO-modeled flow lengths [*Harris and Rowland*, 2001]. Brief showers at rates approaching 10^{-2} mm s^{-1} occur occasionally [e.g., *Blanchard and Spencer*, 1957]. If such a rainfall rate were maintained over the entire length of a channel for the duration of the eruption it would produce an approximately 25% reduction in channel length due to heat lost by vaporizing the rain. Such a situation is extremely unlikely, and would essentially equal the 1-day record for Hawai'i [e.g., *Price*, 1968] (summary available at http://www.ncdc.noaa.gov/oa/climate/extremes/2000/november/extremes1100.html#intro). Note also that for any rainfall-vaporization-derived reduction in length in FLOWGO, the rain must fall on the entire flow for the duration of the eruption. Obviously, heat loss to rainfall is neglected for Mars cases. Heat gain due to latent heat of crystallization typically is on the order of, and often slightly greater than, that lost by radiation. Heat gain due to viscous dissipation is typically negligible.

[7] The governing equation for FLOWGO is that of the mean velocity in a channel (V_c), and is adapted from the Jeffreys equation [*Jeffreys*, 1925; *Moore*, 1987]:

$$V_c = \left(d^2 \rho_{lava} g \sin \theta / 3 \eta_{lava}\right) \Big[1 - (3/2)(YS_{core}/\tau_{base-of-core})$$
$$+ (1/2)(YS_{core}/\tau_{base-of-core})^3\Big]. \qquad (2)$$

In equation (2), YS_{core} is the yield strength of the fluid flow core (that part of the lava that actually deforms), and $\tau_{base-of-core}$ is the amount of shear stress required to deform the lava at the base of the flow core (see *Harris and Rowland* [2001] and *Rowland et al.* [2004] for additional discussion). Note that the starting velocity at the vent is thus a function of channel dimensions, underlying slope, and rheological properties input by the user. Similarly, volumetric flow rate is also a function of these starting parameters and equals $V_c \cdot d \cdot w$, where w is channel width. Unless we have independent knowledge of either channel width or depth at the vent, we set them equal to each other (i.e., the at-vent channel has a square cross section).

FLOWGO holds channel depth constant along its entire length. Because FLOWGO is constrained to conserve mass, this causes channel width to vary when velocity varies (due to downslope changes in rheological properties and/or underlying slope).

[8] The rheological terms in equation (2) are highly dependent on lava temperature [e.g., *Dragoni*, 1989; *Pinkerton and Stevenson*, 1992]. One of the strengths of FLOWGO is that by constantly calculating heat-loss and heat-gain down flow, lava temperature is adjusted at each step and consequently the rheological terms used in the calculation of mean velocity are also adjusted at each step. Another FLOWGO strength is that it accounts for the fact that some of the heat-loss and heat-gain terms are themselves partially dependent on the mean velocity. For example, the percentage of crust on the flow surface affects radiant and convective heat loss, which in turn affects flow velocity, which in turn affects the percentage of cool crust.

[9] FLOWGO determines the maximum distance that lava can flow in a channel for a given set of starting conditions but not the development of the channel itself. Ideally, if any of the following three conditions occur, FLOWGO determines that the lava in the channel has stopped: (1) the velocity becomes zero; (2) the temperature of the flow core reaches that of the solidus; or (3) the yield strength of the flow core (YS_{core}) increases to the point that it equals the shear stress required to deform the base of the flow core ($\tau_{base-of-core}$). In practice, velocity almost always approaches zero (asymptotically, resulting in channel width approaching infinity) before conditions 2 or 3 are reached. Results for the farthest-downflow part of each FLOWGO run are therefore unrealistic. *Lipman and Banks* [1987, Figure 57.18] present cross sections of channel morphology along the 1984 Mauna Loa flow. These show that a distinct channel existed as far as 15 km from the vent and that its width at this point was ~6× that of the near-vent channel. The 1984 channel extended and widened farther downflow, although not diagramed by *Lipman and Banks* [1987]. The near-vent channel of the 1942 Mauna Loa flow was ~20 m wide. A few km from the distal end of the flow, where the channel becomes indistinct, its width is ~200 m [*Rowland*, 2002]. On the basis of these two examples of multikilometer-long, basaltic lava flows we have chosen to consider the distal end of our modeled channel to be the point at which channel width has increased to 10× its at-vent value. Volcanologically, we consider that this stopping point corresponds to the downslope end of a distinct channel. On typical Hawaiian lava flows (basalt) the distal end of the flow is a few km farther downslope, separated from the distinct channel by a zone of dispersed shearing [*Lipman and Banks*, 1987]. In the case of more silicic lava compositions, there is considerably less widening with distance downflow [e.g., *Harris et al.*, 2002] and although not considered in the current treatment, a different definition of the end of the distinct channel would be required.

[10] One of the parameters that FLOWGO calculates is the fraction of surface crust on the top of the flow. This parameter is important because following *Crisp and Baloga* [1990], we model the lava flow surface as a two-component system. These components are incandescent lava at temperature T_{hot} and cooler crust at temperature T_{crust}. Note that T_{hot} is less than the temperature of the flow core (T_{core}), usually by at

least 100°C [*Calvari et al.*, 1994; *Flynn and Mouginis-Mark*, 1994; *Harris et al.*, 1998]. In FLOWGO, f_{crust} is dependent on flow velocity and determined from a relationship derived by analyzing photographs and velocity measurements of the 1984 Mauna Loa channel (see Appendix A).

3. Model Cases and Previous Work

[11] In the analysis that follows we compare Martian and terrestrial cases, incrementally changing planetary parameters to track the changes they produce. Specifically, first we change the gravity term from 9.8 to 3.7 m s^{-2}. Because all other parameters are left unchanged (i.e., they are terrestrial), this is termed the "small-Earth" case. Next we change the ambient atmospheric temperature from +20°C to −63°C, producing a "cold-small-Earth" case. Finally, we replace all atmospheric composition and physical property values with those of Mars to produce a "Mars" case that yields a more complete picture of the Martian effects. In the model runs presented here the properties of the lava are those of the 1984 Mauna Loa flow, a tholeiitic basalt. These properties are summarized in Tables 1 and 2 of *Harris and Rowland* [2001]. All model results were run down a constant 7° slope. Our eventual goal is to apply the Mars-adapted FLOWGO to Elysium Mons to determine probable volumetric flow rates and vent positions. Preliminary results from this effort were reported by *Rowland et al.* [2002] and *Garbeil et al.* [2002].

[12] *Wilson and Head* [1994] published a comprehensive comparison of Martian and terrestrial volcanic processes and expected volcanic features. Briefly summarizing their findings, the major planetary differences that would affect lava flows are the different atmospheric properties and the different gravitational accelerations. The lower atmospheric density on Mars makes heat loss by convection much less efficient than it is on Earth. Thus, although radiative heat loss on the two planets is essentially the same, it dominates total heat loss on Mars to an even greater extent than it does on Earth. Overall, however, they concluded that "...surface cooling differences are not in themselves a significant factor in causing systematic differences between the lengths and widths of lava flows on Mars and the Earth."

[13] Instead, *Wilson and Head* [1994] determined that the Martian condition with the greatest effect will be the lower gravity. They considered that this lower gravity would cause lava to spread laterally to a lesser degree, leading to overall thicker flows for any given rheology. This would reduce the surface-to-volume ratio, which in turn would reduce heat losses, and cause Martian flows to travel farther than their terrestrial counterparts. Our results agree with the idea of the lower gravity on Mars being the dominant factor affecting lava flows relative to those on Earth but as will become clear below, we reach an opposite result, namely that the lower Martian gravity retards the downslope flow of lava, which causes greater cooling per unit distance, and results in shorter flows.

4. Effects of Lower Martian Gravitational Acceleration (the "Small-Earth" Case)

[14] We started with a simple comparison of two flows having the same at-vent channel dimensions and differing
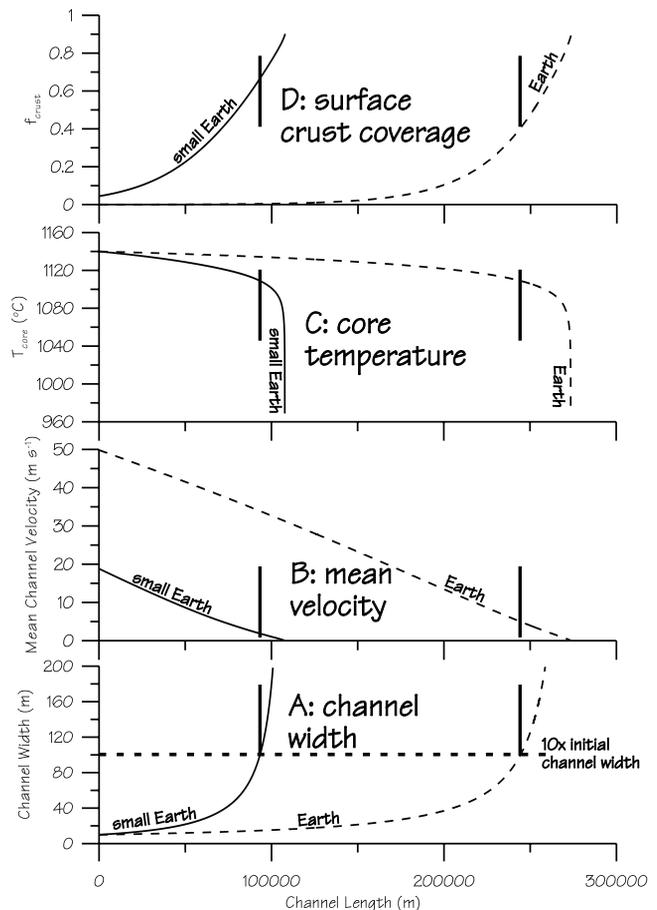
Figure 2. Graphs of (a) channel width, (b) mean velocity, (c) temperature of the flow core, and (d) percent surface coverage by cool crust versus distance down channel for two flows with the same starting width and depth (10 m), using a terrestrial gravity value of 9.8 m s^{-2} (dashed) and a Martian gravity value of 3.7 m s^{-2} (solid); all other parameters are those of Earth. The volumetric flow rate with the Earth gravity is 4983 m^3 s^{-1}, whereas that with the Mars gravity is 1881 m^3 s^{-1}. Vertical black bars indicate distances at which channel width reaches ten times its initial value.

only with respect to the gravitational acceleration. Figure 2 compares downflow variations in channel width, mean channel velocity, the temperature of the flow core, and the percent coverage of the flowing lava by crust for two flows with starting channels 10 m deep by 10 m wide, and gravitational accelerations of 9.8 m s^{-2} and 3.7 m s^{-2}.

[15] Channel width (Figure 2a) increases only slightly along most of the flow distance for both cases. At the distal ends of the flows there is an abrupt widening of the channel, corresponding to the above mentioned asymptotic approach of mean velocity to zero. The black bars indicate 10× the starting channel width and the point beyond which we do not consider our modeled results to be reasonable. Note that all subsequent graphs are clipped at this limit without these bars being shown. Using this limit, the small-Earth channel is ~90 km long compared to a ~240 km-long channel on Earth.
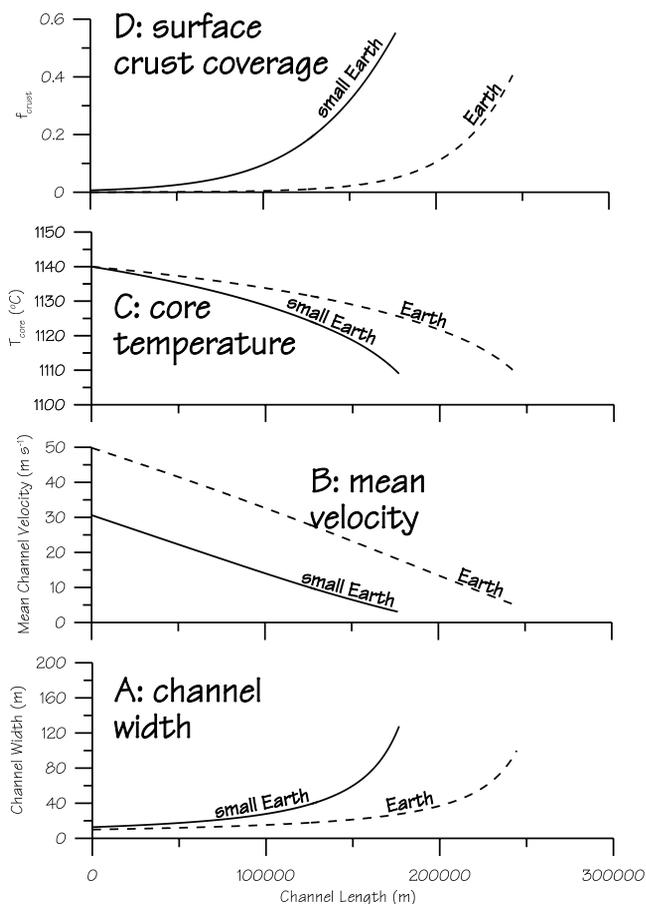
Figure 3. Graphs of (a) channel width, (b) mean velocity, (c) temperature of the flow core, and (d) percent surface coverage by cool crust versus distance down channel for two flows with equivalent volumetric flow rates, with Earth gravity (dashed) and Mars gravity (the "small-Earth" case; solid); all other parameters are those of Earth. At-vent channel depth and width for the Earth case are 10 m, whereas for the small-Earth case they are 12.8 m. The volumetric flow rate for both is 4984 m^3 s^{-1}. Graphs are clipped at the point where channel widths reach $10\times$ their starting values.

[16] The mean small-Earth flow velocity (Figure 2b) at any distance downflow is $\sim$30 m s^{-1} less than the Earth velocity. The temperature of the flow core (T_{core}) for the two flows (Figure 2c) starts at the same value of 1140°C but there is a greater temperature drop per unit distance for the small-Earth lava so that by the point that it has stopped flowing it is $\sim$30°C cooler than lava that has flowed a similar distance in the Earth case. The lower velocity for the small-Earth channel means that the surface crust is not disrupted as much, leading to the result that the percent coverage by such crust (f_{crust}) is always higher for a given distance downflow (Figure 2d).

[17] This initial comparison is less than straightforward because the volumetric flow rates of the two modeled flows differ by more than a factor of two. This is due to the fact that in FLOWGO, neither velocity nor volumetric flow rate are input parameters but instead are consequences of input channel depth, underlying slope, gravity, and terms dealing with lava properties such as density, viscosity, and yield strength (equation (2) and discussion above). Equation (2) shows that all else being equal, the lower value of g for small-Earth will reduce the velocity by 3.7/9.8 ($\sim$60%). If the two channels have the same dimensions, this lower velocity for small-Earth produces a 60% lower volumetric flow rate ($\sim$1800 m^3 s^{-1} versus $\sim$5000 m^3 s^{-1}).

[18] It is more intuitive to compare small-Earth and Earth lava flows at the same volumetric flow rate. To achieve this we determined iteratively the at-vent channel dimensions that would yield a small-Earth flow with a volumetric flow rate equal to $\sim$5000 m^3 s^{-1}. The result of these iterations is a small-Earth channel that has starting depth and width of 12.8 m.

[19] Figure 3 shows the same parameters as Figure 2 but at equivalent volumetric flow rates. There is now less of a difference between the small-Earth and Earth cases. The small-Earth channel is $\sim$175 km long, still about 65 km shorter than the terrestrial channel (Figure 3a) and the mean velocity in the small-Earth channel is $\sim$20 m s^{-1} less than that for the Earth case (Figure 3b). This lower velocity causes the small-Earth channel to be wider at any distance downslope (Figure 3a). For small-Earth, core temperature is always less than (Figure 3c), and surface crust coverage always greater than (Figure 3d), those of Earth, but the differences are smaller than those shown in Figures 2c and 2d, respectively.

[20] The lack of an inverse relationship between core temperature and mean velocity (both are lower in the small-Earth channel than in the Earth channel; Figures 3a and 3c) is perhaps counter-intuitive given that the lower mean velocity for small-Earth results in a greater percentage of (insulating) crust coverage (Figure 3d). Plotting flow variables against time (Figure 4) rather than distance is helpful for illustrating the processes that are occurring. Most obvious is that although lava in the small-Earth channel does not flow as far before it stops, it takes a longer time to flow this shorter distance. Another way to state this is that deceleration in the small-Earth channel is less (Figure 4b). Mean channel velocity for the small-Earth case decreases from 30 to 3 m s^{-1} in 262 minutes (-1.7×10^{-3} m s^{-2}) compared to a decrease from 50 to 5 m s^{-1} in 204 minutes (-3.7×10^{-3} m s^{-2}) in the Earth case.

[21] These relative decelerations mean that although the small-Earth channel is initially wider due to its lower mean velocity, it widens at a slower rate than the Earth channel and at $\sim$140 minutes the two lines cross (Figure 4a). The cooling rate of the small-Earth flow is less (Figure 4c), which is the expected relationship considering its greater rate of surface crust formation (Figure 4d).

[22] The relationships shown in Figures 3 and 4 can be summarized as follows. Because of the difference in gravity, at the same volumetric flow rate the small-Earth lava will flow more slowly and therefore take a longer time to reach any given distance from the vent. Additionally, although the lower velocity allows the small-Earth channel to maintain a more extensive insulating crust, the longer time required to reach a given distance and the greater channel width most of the way (with consequent greater surface area for radiative and convective heat loss) mean that the lava will have cooled to a greater extent by the time it gets there. Ultimately, because at any given distance along the channel
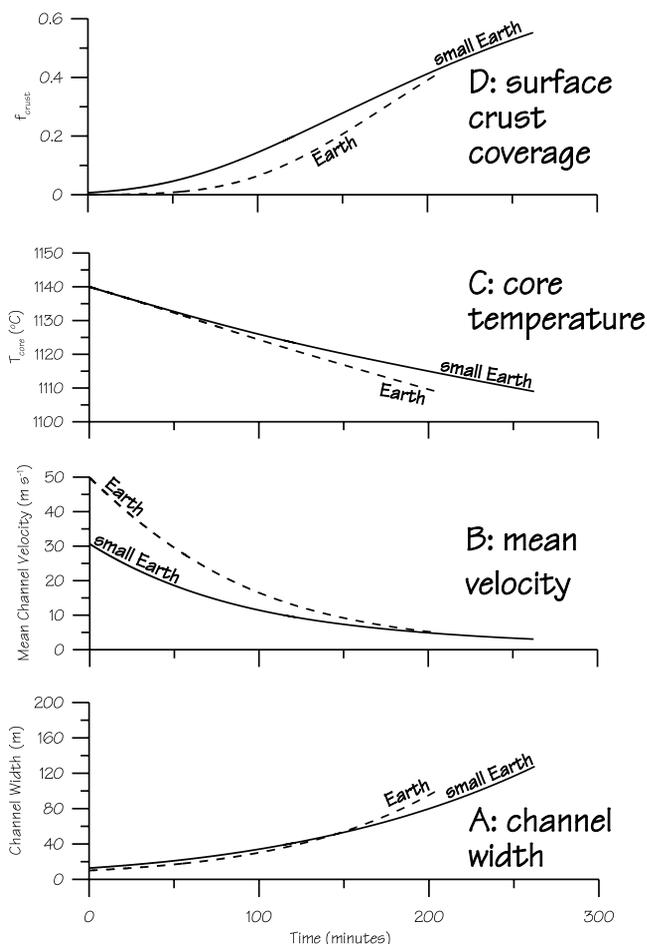
Figure 4. Graphs of (a) channel width, (b) mean velocity, (c) temperature of the flow core, and (d) percent surface coverage by cool crust versus time for two flows with equivalent volumetric flow rates, for the Earth (dashed) and small-Earth (solid) cases; all parameters other than gravity are those of Earth. At-vent channel depth and width for the Earth case are 10 m, whereas for the small-Earth case they are 12.8 m. The volumetric flow rate for both is 4984 m^3 s^{-1}. Graphs are clipped at the point where channel widths reach $10\times$ their starting values.

the small-Earth lava is cooler, its viscosity and yield strength are thus higher than the corresponding Earth lava, causing the flow to slow and eventually stop at a shorter distance from the vent.

5. Effects of a Cold Ambient Atmosphere (the "Cold-Small-Earth" Case)

[23] The comparisons above used an atmospheric temperature of 20°C whereas currently the mean temperature of Mars' atmosphere at the surface is generally around −63°C [e.g., *Ryan and Henry*, 1979] although considerable variations occur with latitude and elevation. Therefore we next examined the effect of a cold atmosphere. Because other atmospheric variables (density, composition, etc.) are still terrestrial, we call this the "cold-small-Earth" case. The red and green lines in Figure 5 correspond to flows that have Mars' gravity and the same 12.8-m starting channel dimen-

sions (and hence volumetric flow rates), but differ with respect to the ambient atmospheric temperature.

[24] The differences between the small-Earth and cold-small-Earth cases are minimal and only discernable beyond ~120 km. Lava flows in the cold-small-Earth channel for ~174 km before the channel width increases 10-fold compared to ~175 km in the small-Earth channel. At these distances the mean velocities are essentially equal (Figure 5b). The cold-small-Earth channel is slightly wider at any given distance downflow (Figure 5a). The differences
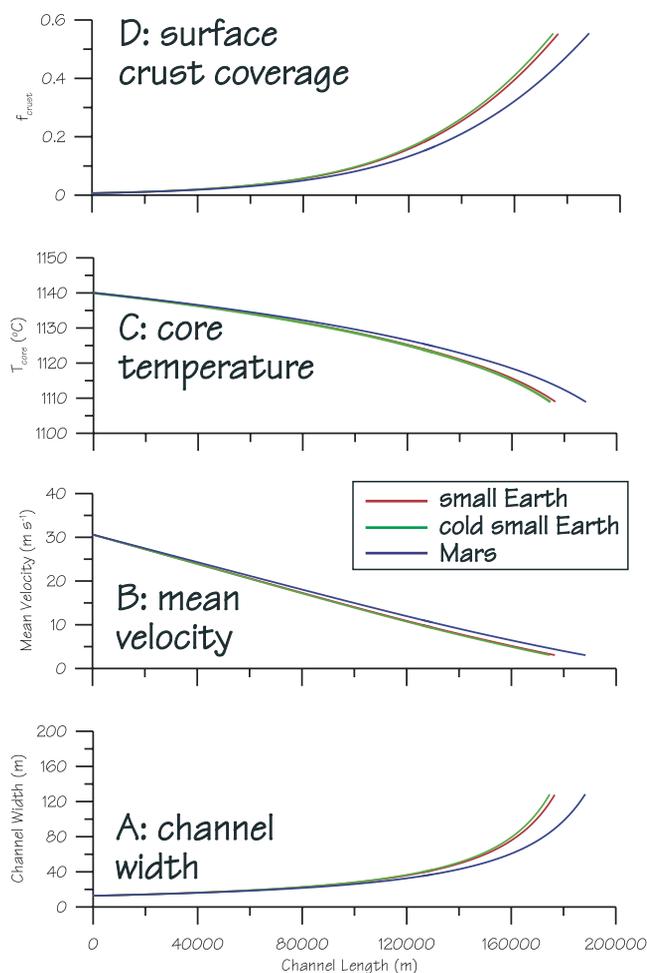

Figure 5. Graphs of (a) channel width, (b) mean velocity, (c) temperature of the flow core, and (d) percent surface coverage by cool crust versus distance down channel for three flows with Mars gravity, starting channel dimensions of 12.8 m × 12.8 m, and volumetric flow rates of 4984 m^3 s^{-1}. "Small-Earth" (red) has an ambient atmospheric temperature of 20°C; other atmospheric properties are those of Earth. "Cold-small-Earth" (green) has an ambient atmospheric temperature of −63°; other atmospheric properties are those of Earth. "Mars" (blue) has an ambient atmospheric temperature of −63°C and uses atmospheric properties calculated for CO_2 under Martian conditions. Note that the change from small-Earth to cold-small-Earth yields a slightly shorter flow, whereas that from cold-small-Earth to Mars produces a longer flow (see text for discussion). Graphs are clipped at the point where channel width reaches $10\times$ its starting value.
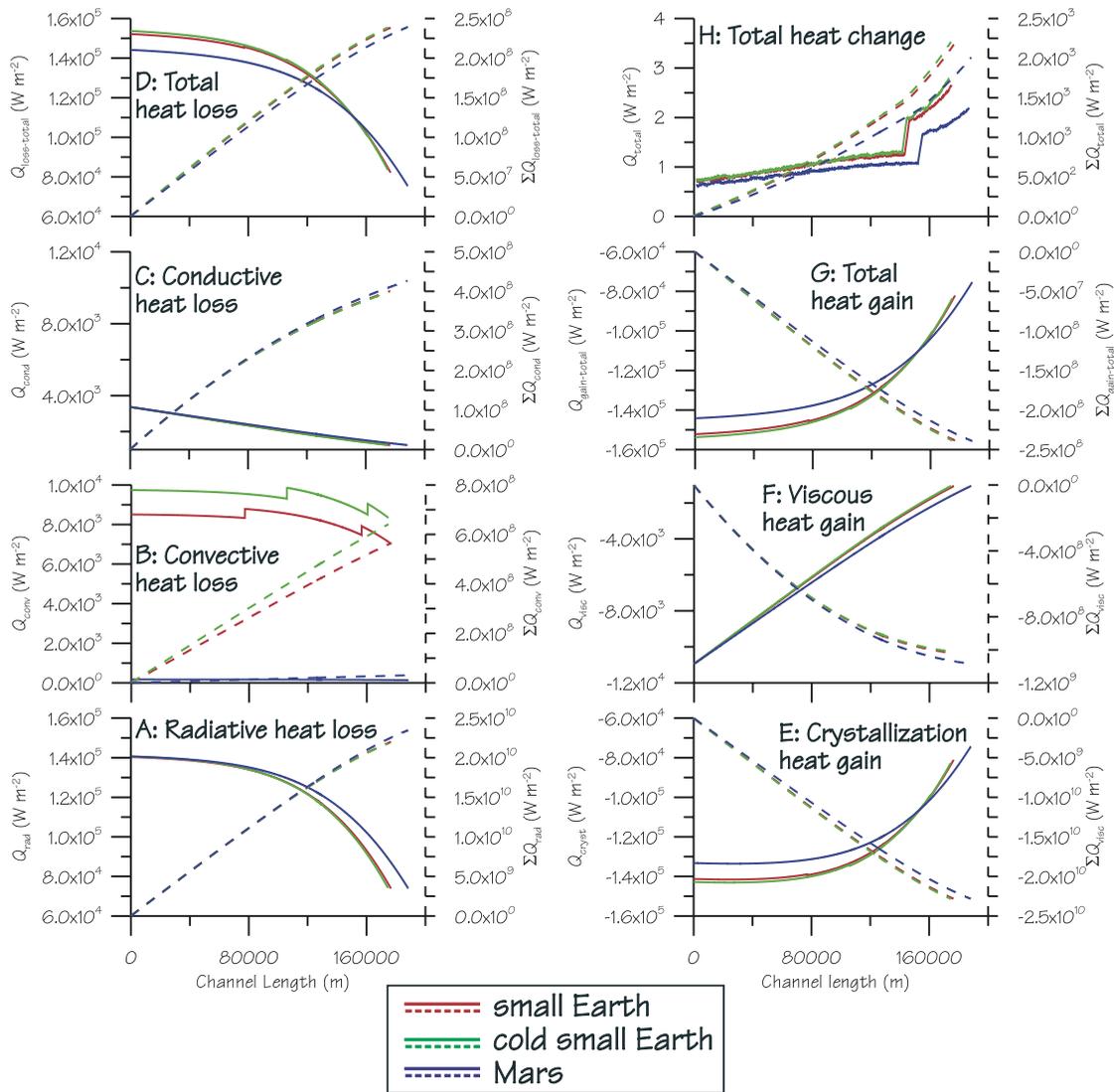
Figure 6. Graphs of individual and summed heat loss and gain terms, for small-Earth (red), cold-small-Earth (green), and Mars (blue). Solid lines are heat losses at each location down-channel and dashed lines are cumulative heat loss down channel. Note that heat lost to convection (Figure 6b) shows the greatest amount of variation among cases. In particular, cold-small-Earth has slightly more convective heat loss than small-Earth, whereas Mars has significantly less convective heat loss than both small-Earth and cold-small-Earth (accompanied by a switch of convective heat loss dominance from forced to free; see text). In the plot of total heat change (Figure 6h), the jump in all three plots at a channel length of ~140,000 m is due to a change in crystallizing phase at 1200°C in the MELTS program [*Ghiorso and Sachs*, 1995], which FLOWGO uses to determine latent heat of crystallization. Note that this jump is evident only in Figure 6h because of its much reduced vertical scale compared to Figures 6a–6g. Graphs are clipped at the point where channel width reaches 10× its starting value.

in T_{core} and f_{crust} are similarly slight, becoming apparent only near the downflow end of the channels. The temperature-induced change from small-Earth to cold-small-Earth therefore produces differences of the same sense but of considerably smaller magnitude than the gravity-induced changes from Earth to small-Earth.

[25] These results indicate that greater heat loss is occurring because of the colder atmosphere, producing lower flow core temperatures and greater fractional coverage by surface crust. Although slight, the differences between the small-Earth and cold-small-Earth cases are useful for illus-

trating the interactions between heat loss processes, rheology, and the distance that lava can flow down a channel.

[26] Almost all of the increased heat loss that occurs when the ambient temperature is reduced is due to increased convection (Figure 6b). Following *Head and Wilson* [1986], FLOWGO utilizes the greater of free or forced convection in its calculation of overall heat loss, and which of these terms dominates is determined by the input wind speed. Average wind speeds measured by the Viking landers were $5–10$ m s^{-1} in the summer and $2–7$ m s^{-1} in winter [*Hess et al.*, 1977; *Ryan et al.*, 1978]. More recently the Mars

Pathfinder windsock experiment recorded wind speeds that were commonly <8 m s^{-1} with a maximum recorded gust of 12 m s^{-1} [*Sullivan et al.*, 1998]. We used a wind speed value of 5 m s^{-1} for all the FLOWGO results presented here. Using this, forced convection is always ∼2.5 times greater than free convection along the entire channel length for both the small-Earth and cold-small-Earth cases. Higher wind speeds are possible, for example during dust storms, and these would cause increased convective cooling and shorter lava flows. We found that for the cold-small-Earth case (and holding all other factors equal), each 5 m s^{-1} increase in wind speed shortens the modeled distance that the lava can flow by ∼10 km. As with the rainfall discussion above, these results assume that the wind speed increases are applied along the entire flow length for the duration of the eruption.

[27] Heat lost to forced convection (Q$_{force}$) is given by [e.g., *Keszthelyi and Denlinger*, 1996]

$$Q_{force} = U \, C_H \, \Delta T_{surf} \, \rho_{atmos} \, cp_{atmos}. \qquad (3)$$

Q$_{force}$ varies directly with ΔT_{surf} (the difference between the effective lava surface temperature and the ambient atmospheric temperature), wind speed (U; 5 m s^{-1}), and a wind friction factor (C$_H$) which is equal to 0.0036 [*Greeley and Iverson*, 1987; *Keszthelyi and Denlinger*, 1996]. Q$_{force}$ also varies directly with ρ_{atmos} and cp$_{atmos}$, respectively the density and heat capacity of the air immediately adjacent to the lava surface. Both ρ_{atmos} and cp$_{atmos}$ are temperature-dependent and change as the flow surface cools. For a terrestrial atmosphere, which is the situation both for small-Earth and cold-small-Earth cases, FLOWGO uses look-up tables [*Kays and Crawford*, 1980] to derive these temperature-dependent values. The discontinuities in the convective heat loss graph (Figure 6b) are due to changes in the look-up tables for values of ρ_{air} and cp$_{air}$ at particular temperature thresholds.

[28] From small-Earth to cold-small-Earth, the ΔT_{surf} term increases by 83°C, favoring a larger value for Q$_{force}$. This is enhanced by the fact that as the ambient temperature decreases, both ρ_{atmos} and cp$_{atmos}$ also increase (see Appendix A). This increased convective heat-loss decreases the flow core temperature slightly, leading to slight increases in both the viscosity and yield strength at every point along the flow. These in turn reduce the mean velocity via equation (2).

[29] Radiative heat loss (Q$_{rad}$) is calculated after *Crisp and Baloga* [1990] and *Oppenheimer* [1991] from

$$Q_{rad} = \sigma \, \varepsilon \{ f_{crust} [T_{crust}^4 - T_{ambient}^4] + (1 - f_{crust}) [T_{hot}^4 - T_{ambient}^4] \}. \qquad (4)$$

In equation (4), σ is the Stephan-Boltzmann constant, ε is the emissivity of basalt, and T$_{crust}$, T$_{hot}$, and T$_{ambient}$ are the temperatures of the cool surface component, hot surface component, and ambient atmospheric temperature, respectively. The lower atmospheric temperature (by 83°C) of the cold-small-Earth case means that both the $[T_{crust}^4 - T_{ambient}^4]$ and $[T_{hot}^4 - T_{ambient}^4]$ terms are larger than they are for the small-Earth case, leading to an increase in heat lost to radiation. However, because T$_{crust}$ and T$_{hot}$ are so much greater than T$_{ambient}$, this increase is very slight and the

flow-length decrease due to increased radiative heat loss is negligible (Figure 6a). The slight offset between small-Earth and cold-small-Earth seen in Figure 6a is almost all horizontal (as opposed to the vertical offset in Figure 6b) and is caused by the slightly shorter length of the cold-small-Earth flow.

[30] The equation for Q$_{cond}$, the heat lost by conduction into the levees and underlying pre-eruption surface [after *Bird et al.*, 1960; *Keszthelyi and Self*, 1998] is

$$Q_{cond} = \alpha_{lava} (\Delta T_{base} / H_b). \qquad (5)$$

Here, α_{lava} is the thermal conductivity of basalt, ΔT_{base} is the temperature difference between the flow core and the pre-eruption surface, and H$_b$ is the thickness of the flow base. Note that atmospheric temperature does not occur in equation (5). In addition to the atmosphere being colder, however, the surface of Mars is typically colder than that of (most of) the Earth. FLOWGO models lava flowing in an established channel, meaning we assume that the underlying surface has been heated by the active flow to a constant temperature, which on Earth we take to be 700 ± 200°C [*Keszthelyi*, 1995b; *Wooster et al.*, 1997]. If the starting temperature of the Martian ground surface is colder, then the surface under an active channel will also be colder, and ΔT_{base} will therefore be larger. *Kieffer et al.* [1977] show that typical pre-dawn (coldest) temperatures on the upper flanks of Martian volcanoes range between −30 and −20°C. To assess the effects of a colder substrate, we decreased the temperature of the underlying surface (i.e., increased ΔT_{base}) by increments of 50°C. This resulted in slightly increased values of Q$_{cond}$ with consequent very minor decreased flow lengths (∼2 km per 50°C increase in ΔT_{base}). This channel length increase is insignificant considering the flow-length variations that result from uncertainties in at-vent rheological values. The increase is even more negligible because conductive heat losses over the temperature range we are concerned with are small to begin with (compare the left-hand vertical scale of Figure 6c to that of other plots in Figure 6). The overall results agree with *Hulme* [1982] and *Wilson and Head* [1994], both of whom considered conductive heat losses on Earth and Mars to be essentially the same.

[31] We do not consider thermal erosion by the channel because of the short times being modeled. *Kauahikaua et al.* [1998] studied lava flowing in a tube on Kīlauea and measured a downcutting rate of ∼10 cm d^{-1} over a period of months. They estimated that this downcutting probably started 1−2 days after the lava tube formed. Figure 4 shows that our modeled flows stop after ∼260 minutes (∼4 hours), during which time downcutting, if any, would be minimal. This does not mean that thermal erosion does not occur during a Martian eruption. Recall that FLOWGO does not model the emplacement of the flow, but instead the ability of an element of lava to travel down an established channel. Thus, although such an element of lava will take ∼4 hours to travel the entire channel length and in that time not contribute (and therefore lose) appreciable heat to thermal erosion, over the duration of the entire eruption, thermal erosion might very well occur [e.g., *Wilson and Mouginis-Mark*, 2001].

[32] Heat gained by viscous dissipation (Q_{visc}) is calculated from *Costa and Macedonio* [2003]:

$$Q_{visc} = \eta_{lava}(V_c/d)^2. \qquad (6)$$

Although atmospheric temperature does not appear in equation (6), there are two terms, velocity (V_c) and dynamic viscosity (η_{lava}), that are different in the cold-small-Earth case relative to the small-Earth case because of the above mentioned increased convective cooling due to the colder atmosphere. Dynamic viscosity increases because the increased convective heat loss lowers the lava core temperature (T_{core}). The temperature-controlled viscosity increase relies on an $\exp[\omega(T_{erupt} - T_{core})]$ term, where ω is a constant and T_{erupt} is the starting temperature of the flow core [*Dragoni*, 1989; *Pinkerton and Stevenson*, 1992]. Note that a decrease in T_{core} causes the exponent term to increase, however, it is by an exceedingly small amount (a difference of 0.0001 by the end of the channel). The resulting exceedingly small increase in dynamic viscosity causes a decrease in channel velocity (V_c; equation (2)). Note that V_c is squared in equation (6), so its decrease negates the increase in dynamic viscosity. The colder atmosphere thus induces small and opposite effects on Q_{visc}, resulting in a negligible overall change.

[33] Heat gained by latent heat of crystallization (Q_{cryst}) is calculated after *Marsh* [1981] and *Crisp and Baloga* [1994] from

$$Q_{cryst} = (\delta T_{core}/\delta x) \, E_r \, \rho_{lava} \, L_{cryst}\left(\delta\varphi_{cryst}/\delta T_{core}\right), \qquad (7)$$

where $\delta T_{core}/\delta x$ is the change in flow core temperature with distance, E_r is the volumetric flow rate, L_{cryst} is the latent heat of crystallization, and $\delta\varphi_{cryst}/\delta T_{core}$ is the change in volume percent crystals per degree of flow core cooling [*Crisp and Baloga*, 1994; *Harris and Rowland*, 2001]. Figure 5c shows that there is a very slightly greater drop in core temperature per distance for cold-small-Earth than there is for small-Earth. This corresponds to the $\delta T_{core}/\delta x$ term in equation (7) being slightly greater for cold-small-Earth and means that there is a little more heat gained by crystallization in this case. Recall that FLOWGO conserves volumetric flow rate so that even though the mean velocity of the cold-small-Earth flow is a little less at any given distance than that of the small-Earth flow, E_r is the same for the two flows. The lower temperature therefore only affects the $\delta T_{core}/\delta x$ term (leading to increased Q_{cryst}), but as shown in Figure 6e, the effect is very slight.

[34] Figure 6 compares all the heat loss and heat gain terms for the small-Earth (red) and cold-small-Earth (green) cases. Note that the values for heat gain are plotted with the opposite sign than those of heat loss (a larger negative number for heat gain means more heat gain). The only meaningful heat loss difference is that for convection (Figure 6b), with the cold-small-Earth flow losing ~1200 W m^{-2} more at every point downflow. Radiative heat loss is increased very slightly due to the colder atmosphere and conductive heat loss is increased by an even smaller amount by the related colder surface temperature. Combined, these result in slightly greater total heat loss due to the colder ambient temperature. The

colder ambient temperature reduces heat gained by viscous dissipation by a very small amount but increases that gained by latent heat of crystallization, by a slightly greater amount. Overall, therefore, the colder ambient temperature results in slightly more heat gained as the lava flows down the channel.

[35] Thus both total heat loss and total heat gain are increased slightly by lowering the ambient atmospheric temperature (Figures 6d and 6g). Although the two terms are almost equal (note the vertical scale in Figure 6h), for the cold-small-Earth case relative to the small Earth case, the sum of heat losses is at all points slightly greater than the sum of heat gains. Similar to the situation when velocity decreases (due to gravity being reduced from 9.8 to 3.7 m s^{-2}), the velocity decrease due to increased cooling causes the lava to lose more heat per unit distance downflow. The result is that it cannot flow as far, but the effect is significantly smaller than that caused by reducing gravity.

[36] A careful reader will notice that the heat loss and heat gain equations presented here differ from those in the original FLOWGO paper by the absence of the flow width term, w [*Harris and Rowland*, 2001, Table 3]. The heat losses and gains in the original FLOWGO paper are with respect to the 1-m downflow increments that the model utilizes. Including this width term presents two problems in the current work. The first is that the resulting heat loss or gain units are W m^{-1}, rather than the more familiar W m^{-2}. The second is that as the lava slows, the channel width increases, resulting in increased heat losses and gains when summed across the channel width. It is counter-intuitive that heat loss and gain should increase as a flow cools and comes to a stop. The solution to both problems is to divide all the FLOWGO-derived heat loss and gain values by flow width, resulting in the formulae presented here.

6. Effects of a Martian Atmosphere (the "Mars" Case)

[37] Our final analysis examines the effects of the low density and almost wholly CO_2 composition of the Martian atmosphere. When these atmospheric parameters are included (along with the lower gravity and atmospheric temperature) we are replicating, to the extent that FLOWGO allows, a complete "Mars" case. FLOWGO uses a number of atmospheric values when calculating heat loss, all of which refer to the boundary layer between atmosphere and lava surface and therefore occur in the equations for forced and free convection. These are density (ρ_{atmos}), dynamic viscosity (η_{atmos}), kinematic viscosity (ν_{atmos}), thermal conductivity (α_{atmos}), heat capacity (cp_{atmos}), thermal diffusivity (β_{atmos}), and cubic expansivity (κ_{atmos}). The original FLOWGO program uses a set of look-up tables derived from *Kays and Crawford* [1980] to adjust the relevant (terrestrial) atmospheric values as they vary with temperature. We were unable to find equivalent tables for the Martian atmosphere or for pure CO_2 and instead built into FLOWGO the ability to calculate these parameters directly at each increment down the channel, using theoretical thermophysical relationships [e.g., *Adamson*, 1979] (Chemical Properties Handbook Web site: http://www.knovel.com/knovel2/default.jsp). Details of these calculations are presented in Appendix A. An added benefit to this
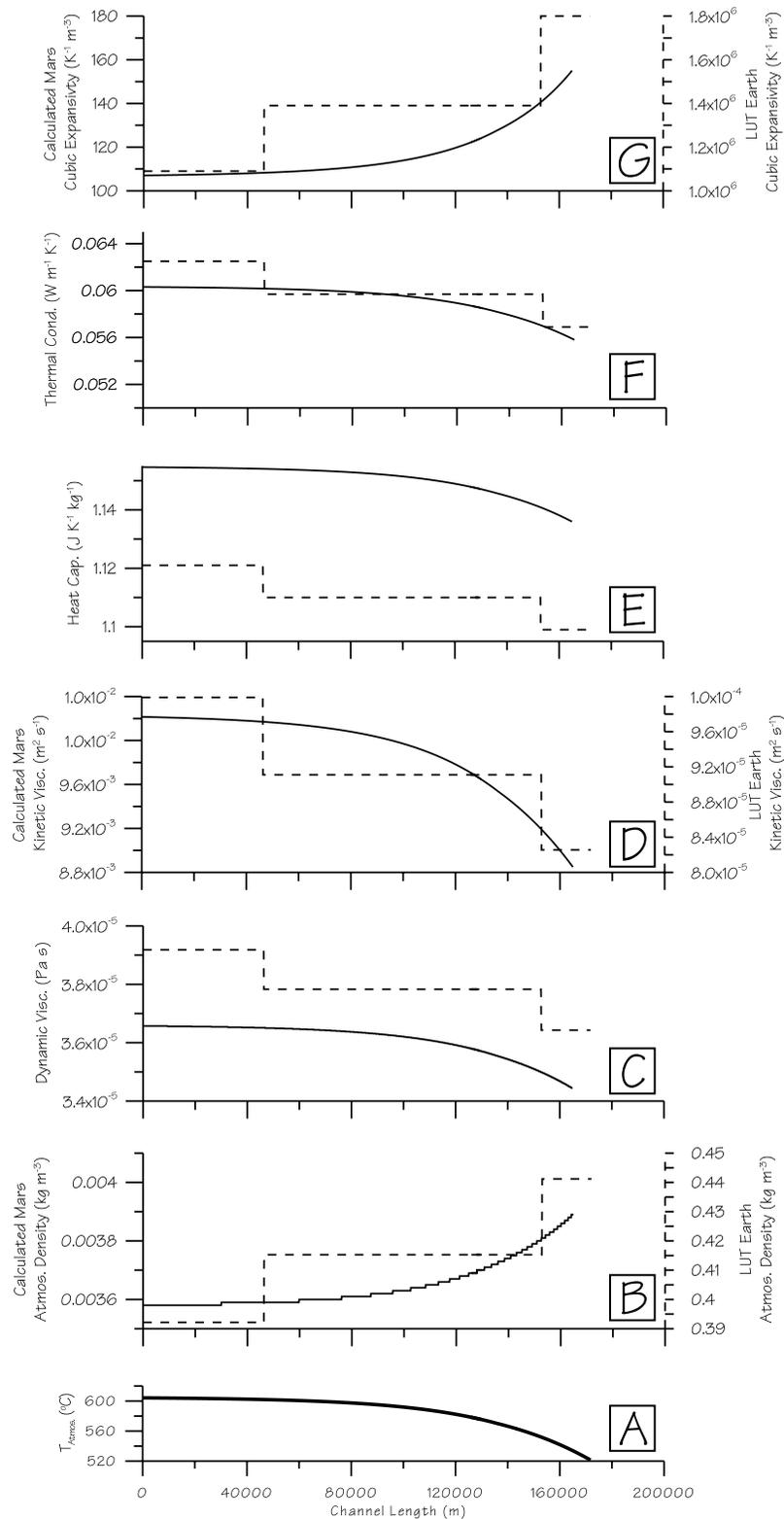
Figure 7. Graphs of Martian (solid; calculated by FLOWGO) and terrestrial (dashed; from look-up tables) atmospheric variables. Vertical scales are the same unless there is a significant difference in the values (density, kinematic viscosity, and cubic expansivity).

approach is that it avoids the discontinuities in FLOWGO results that result from discontinuities in the look-up tables.

[38] Figure 7 compares, along the length of our test flow, FLOWGO-calculated and look-up-table-derived atmospheric properties. These include a gravity value of 3.7 m s^{-2} and an ambient atmospheric temperature of $-63°$C, and therefore compare the cold-small-Earth atmosphere to the Mars atmosphere. All of the properties are

dependent on T_{atmos}, the average of the ambient atmospheric temperature and the effective lava surface temperature (which in turn depends on the relative areas of cool crust and hot cracks; Appendix A). Figure 7a shows that T_{atmos} remains relatively constant for about half the channel length before starting to drop. The calculated Martian atmospheric density is lower by more than two orders of magnitude (Figure 7b), mainly because the Martian atmospheric pressure is so much lower than on Earth (600 versus 1.03 × 10^5 Pa [Hess et al., 1977; Ryan et al., 1978]). Because they involve atmospheric density, kinematic viscosity and cubic expansivity also differ significantly between cold-small-Earth and Mars cases. Kinematic viscosity (Figure 7d) for Mars is ∼2 orders of magnitude greater than for cold-small-Earth. Cubic expansivity (Figure 7g) for a Mars atmosphere is ∼4 orders of magnitude less than that for cold-small-Earth.

[39] With respect to cold-small-Earth, dynamic viscosity for Mars is slightly lower (Figure 7c) and specific heat capacity is slightly higher (Figure 7e). Thermal conductivity (Figure 7f) is essentially the same for the two atmospheres. Thermal diffusivity is T_{atmos}^{-1} and therefore doesn't change between cold-small-Earth and Mars.

[40] These atmospheric variables occur only in the heat-loss formulae for forced and free convection [e.g., Keszthelyi and Denlinger, 1996]:

$$Q_{force} = U \ C_H \ \Delta T_{surf} \ \rho_{atmos} \ cp_{atmos}, \qquad (3)$$

$$\begin{aligned} Q_{free} = 0.14 \ \alpha_{atmos} (g \ \kappa_{atmos} \ \rho_{atmos} / \eta_{atmos} \ \beta_{atmos})^{1/3} \\ \cdot (T_e - T_{atmos})^{4/3}. \end{aligned} \qquad (8)$$

[41] Recall from above that in equation (3), U is wind speed (which we hold constant at 5 m s^{-1}), C_H is a wind friction factor equal to 0.0036 [Greeley and Iverson, 1987; Keszthelyi and Denlinger, 1996], and ΔT_{surf} is the difference between the effective lava surface temperature and the ambient atmospheric temperature. Although cp_{atmos} for Mars is slightly greater than that for cold-small-Earth (Figure 7e), the much lower ρ_{atmos} term dominates, causing Q_{force} for Mars to be considerably lower.

[42] In equation (8), T_e is the effective surface temperature (see Appendix A) and T_{atmos} is the average between the ambient atmospheric temperature ($T_{ambient}$) and T_e; neither of these terms differs between cold-small-Earth and Mars. Two terms in equation (8) that do have considerably different values in the cold-small-Earth and Mars cases are ρ_{atmos} and κ_{atmos}. Both terms are much lower in the Mars case and both are in a numerator, suggesting that Q_{free} will decrease in the Mars case relative to the cold Earth case. This decrease is moderated, however, because this numerator is part of a term that is reduced by a 1/3 power. The overall result is that relative to cold-small-Earth, the decrease of Q_{free} in the Mars case is smaller than the decrease of Q_{force}. Thus, unlike both the small-Earth and cold-small-Earth cases, Q_{free} is the dominant convective heat loss mechanism for Mars, maintaining a value of ∼2 × Q_{force} along the entire channel length.

[43] Q_{free} for the Mars case is considerably less than Q_{force} for the small-Earth and cold-small-Earth cases (Figure 6b). In fact, convective heat loss becomes essen-tially negligible, which also agrees with the results of Wilson and Head [1994]. As noted above, equation (7) for heat gained by latent heat of crystallization, contains a term for temperature decrease with distance ($\delta T_{core}/\delta x$). Figure 5c shows that $\delta T_{core}/\delta x$ is less for Mars and this reduces the amount of heat gained by latent heat of crystallization relative to the cold-small-Earth case.

[44] Radiative and conductive heat loss are not affected by the change to Martian atmospheric properties. In Figures 6a and 6c, only horizontal offsets occur between the Mars case and the cold-small-Earth cases. The change to Martian atmospheric parameters therefore only produces direct heat changes in convective heat loss (reduced, favoring a longer flow; Figure 6b) and latent crystalliza-tion heat gain (reduced, favoring a shorter flow; Figure 6e). The convective effect is greater, leading to slightly lower overall heat loss (Figure 6h), and in turn resulting in a longer flow.

[45] The blue lines in Figure 5 show the resulting channel parameters for the Mars case. Specifically, the ability to flow farther (because of reduced convective cooling) man-ifests as slight horizontal and vertical offsets toward longer flows with respect to channel width, mean velocity, flow core temperature and surface crust coverage.

[46] Thus, unlike the change from the small-Earth case to the cold-small-Earth case, wherein overall heat loss increased (although only slightly) and led to a slightly shorter flow, the change from the cold-small-Earth case to the Mars case results in a reduction of overall heat loss and therefore a longer flow. The Mars case channel extends almost to 190 km before the 10× initial channel width cut-off, an increase of ∼15 km over the cold-small-Earth case. However, this 190 km-length remains ∼60 km shorter than a terrestrial flow with the same volumetric flow rate (compare Figures 5 and 3, noting that the horizontal axes are not the same).

7. Discussion

[47] Our results show that an eruption with an effusion rate of ∼5000 m^3 s^{-1} under Mars' gravitational and atmospheric conditions would allow lava to flow in a channel for almost 190 km on an underlying slope of 7° (the Mars case presented above). Such slopes are common on Elysium Mons volcano [Kallianpur and Mouginis-Mark, 2001]. The distinct channel would then transition into a zone of shearing and then into a zone of dispersed flow at the distal end [Lipman and Banks, 1987]. Thus the entire flow length (channelized and unchannelized portions combined) could reach 200 km. Mouginis-Mark and Tatsumura-Yoshioka [1998] mapped 59 lava flows on Elysium Mons. The mapped lengths of most of these Elysium Mons flows are <150 km although none of the flows could be traced back to their source vents so the reported lengths are minima. We consider it reasonable therefore that the eruption conditions presented in the Mars case could have produced most of the flows mapped on Elysium Mons by Mouginis-Mark and Tatsumura-Yoshioka [1998].

[48] Rowland et al. [2004] discuss the relationship between "effective" volumetric flow rates, those that replicate known flow lengths, and the maximum volumetric

flow rates associated with these flows. Basically, maximum volumetric flow rates occur early in an eruption [e.g., *Wadge*, 1981; *Crisp*, 1984; *Harris et al.*, 2000], but at this point there has not been enough time to develop a long channel. Later, when the channel has developed its maximum length downslope (and thereby made it more efficient for lava to travel downslope), the volumetric flow rate has decreased. On the basis of the 1984 Mauna Loa example, the FLOWGO-derived effective volumetric flow rate that produced a channel length equal to that measured in the field was $\sim$200 m^3 s^{-1}. This compares to a maximum volumetric flow rate that was probably between 300–500 m^3 s^{-1} during the first few hours of the eruption [*Lipman and Banks*, 1987; *Rowland et al.*, 2004]. Considering all the uncertainties in these numbers there is roughly a factor of two difference between the effective and maximum volumetric flow rates. The volumetric flow rate used in the model results presented here is likewise an "effective" value and therefore would correspond to a maximum volumetric flow rate (i.e., early in a Martian eruption) of $\sim$10,000 m^3 s^{-1}. The largest volumetric flow rate for a historical basaltic eruption is that of the Icelandic volcano Laki during the years 1783–1785 [*Thordarson and Self*, 1993], with a calculated maximum volumetric flow rate of 8500–8700 m^3 s^{-1}. These comparisons indicate that volumetric flow rates for Elysium Mons lava flows need not be considerably higher than those that have occurred recently on Earth.

[49] One of our results is that the lower gravitational acceleration on Mars contributes to lava flowing a shorter distance than on Earth. This is the case even when the Martian volumetric flow rate is increased to that of the modeled Earth flow (which, in FLOWGO, is achieved by increasing the channel dimension). Martian lava flowing a shorter distance due to lower gravity is a result opposite of that reached by *Wilson and Head* [1994]. As noted above, the gravitational effect they considered is the lateral spreading of lava as it flows, and more fundamentally, how the ratio of surface area to volume affects heat loss. In their treatment, lateral spreading is taken into account by one of the rheological terms, $[YS_{lava}/\rho_{lava} g]^{6/11}$, within a formula for flow length [from *Pinkerton and Wilson*, 1994] that also includes terms for Gratz number, effusion rate, and underlying slope. Because the gravity term is in the denominator, reducing it increases the value of that particular rheological term and hence the calculated lava flow length.

[50] In one sense these results may not be as contradictory as they initially appear because different parts of the lava flow are being considered in the two treatments. *Wilson and Head* [1994] considered processes that determine the initial thickness and width of a lava flow lobe. It is within this initial lobe that a channel (the part considered by FLOWGO) will develop. The two parts of the flow are clearly related because the dimensions of the channel are a function of the flow lobe within which it develops [e.g., *Hulme*, 1974]. Thus our need to deepen and widen the channel in order to produce a terrestrial volumetric flow rate may account for the lower-gravity-derived thicker flow. On the other hand, even with this deeper and wider Martian channel, lava still doesn't flow as far as it does in the terrestrial channel.

[51] We do not equalize the volumetric flow rate by increasing the at-vent channel depth only (leaving at-vent width unchanged). This is because FLOWGO is very sensitive to channel depth and the result would be to produce a considerably longer flow (all other parameters being equal). We prefer to use an equidimensional at-vent channel unless we have independent knowledge of either width or depth, because this requires the fewest a priori assumptions and because near-vent channels during the 1984 Mauna Loa eruption were nearly equidimensional [*Lipman and Banks*, 1987]. A fully developed flow model that allows gravitational effects to actually derive at-vent flow-lobe dimensions and in turn, channel depth and width (along with contributions from eruption conditions, rheology, slope, etc.) is required to resolve these issues of the overall gravitational effect but this is currently beyond the capability of FLOWGO.

[52] Finally, the data in Figure 6 allow us to examine the interplay between the heat loss and gain processes that occur as lava flows in a channel. In particular, it is interesting to note that for the small-Earth and cold-small-Earth cases, the most significant heat gain term (Q_{cryst}) is actually greater at any distance down flow than the most significant heat loss term (Q_{rad}). The significant role of latent heat of crystallization was emphasized by *Crisp et al.* [1994] and *Crisp and Baloga* [1994] and, clearly, ignoring this term will lead to incorrect results. Additionally, the other heat gain term Q_{visc}, although small, is greater than conductive heat loss, Q_{cond}. Considering only these four heat change terms would result in a flow that heats up as it flows and therefore would never stop. The remaining heat loss term, Q_{conv}, tips the balance in favor of heat loss dominance which is required if a cooling-limited flow is going to stop.

[53] For Mars, the Q_{conv} heat loss term disappears almost entirely (Figure 6b), reducing total heat loss (Figure 6d). At the same time, the Q_{visc} heat gain term increases slightly (Figure 6f). Together these would produce a flow that heats up as it flows were it not for the fact that the Q_{cryst} heat gain term (Figure 6e) is reduced enough that total heat loss is always greater. Figure 6h shows that there is an even closer balance between total heat loss and heat gain for the Mars case.

[54] Comparing the vertical scale of the overall heat change graph (Figure 6h) with those of all the other heat loss and gain terms shows that there is nearly a balance between heat loss and gain. We consider this to be reasonable because in the absence of super heat, crystallization will occur every step of the way. Heat lost by radiation, convection, and conduction therefore results in crystallization which, in turn, produces latent heat which moderates the heat lost. This set of processes only occurs if crystallization can occur rapidly such as in low-viscosity lavas. The low viscosity of basalt therefore not only allows the lava to flow easily, it also allows crystallization to occur easily and this, in turn, releases latent heat which keeps the flow hot for a longer time. Indeed, as *Marsh* [1981] points out, the crystallization of a pure solid under ideal conditions is isothermal. In evolved lava compositions, however, the high viscosity impedes crystallization. This results in considerably less latent heat of crystallization being generated, and the overall heat balance swings

strongly to heat loss. This lack of a heat-loss buffer augments the resistance to flow due to high viscosity and yield strength, and contributes to the inability of silicic flows to flow very far.

8. Conclusions

[55] In conclusion, we have examined the ways in which eruption in a Martian environment will affect the flow of lava in a channel. The greatest difference between a Martian flow and an equivalent terrestrial flow is due to the lower gravitational acceleration on Mars. This causes the Martian lava to flow more slowly and in so doing, cooling is able to occur to a greater degree along each downflow increment. The result is that the Martian lava is unable to flow as far as its Earth counterpart and it takes a longer time to attain its shorter distance. Including the effects of the cold Martian atmosphere shortens the flow even more by increasing heat lost by convection but the effect is miniscule. Finally, using an atmosphere with physical and chemical properties more realistic for Mars (essentially low-density CO_2) decreases heat loss by convection which allows the lava to flow farther than if terrestrial atmospheric properties are assumed. This decreased heat loss favors increased channel length but does not compensate for the flow-length decrease caused by the lower gravity.

[56] The result is that lava flowing at the same volumetric flow rate will not travel as far on Mars as it will on Earth. However, volumetric flow rates required to produce some of the long lava flows observed on Mars [e.g., *Mouginis-Mark and Tatsumura-Yoshioka*, 1998] are not enormously higher than the maximum values recorded on Earth.

Appendix A

[57] The following presents the formulae used to determine Martian atmospheric values used by FLOWGO in its calculation of heat loss by convection (equations (3) and (8); Figure 7). We have approximated the Martian atmosphere as pure CO_2. The values to consider are density, dynamic viscosity, kinematic viscosity, thermal conductivity, heat capacity, thermal diffusivity, and cubic expansivity.

[58] Density (ρ_{atmos}) was determined from the ideal gas law:

$$\rho_{atmos} = P_{Mars} \, T_{atmos}^{-1} \, R_{Mars}^{-1}. \tag{A1}$$

We used pressure at the Mars datum (600 Pa), an ideal gas constant, R_{Mars}, of 0.19 J mol^{-1} K^{-1} (M. Smith, personal communication, 2003), and T_{atmos}, the average of the ambient atmospheric and effective lava surface temperatures ($T_{ambient}$ and T_e, respectively) at each downflow step:

$$T_{atmos} = 1/2(T_e + T_{ambient}). \tag{A2}$$

$T_{ambient}$ is $-63°C$, and T_e is the effective temperature of the lava surface based on the relative amounts of exposed

hot and crusted lava. It is calculated at each downflow step [*Crisp and Baloga*, 1994] from

$$T_e = \left[f_{crust} \, T_{crust}^4 + (1 - f_{crust}) T_{hot}^4 \right]^{1/4}. \tag{A3}$$

[59] The fractional coverage by crust is velocity-dependent and is also calculated at each downflow step, from an empirical relationship (with a correlation coefficient of 0.9 [*Harris and Rowland*, 2001]) that is based on estimates of crust coverage in photographs and flow velocity data, both given by *Lipman and Banks* [1987]:

$$f_{crust} = 0.9 \exp[-0.16 \, V_c]. \tag{A4}$$

Dynamic viscosity (η_{atmos}) was determined from a gas viscosity calculator available at http://www.lmnoeng.com/Flow/GasViscosity.htm which uses Sutherland's formula, as presented by *Crane Company* [1988]:

$$\eta_{CO2} = \eta_{0atmos}(a/b) \, (T_{atmos}/T_0)^{3/2}, \tag{A5}$$

where η_{0atmos} is the reference dynamic viscosity for CO_2 (1.48×10^{-5} Pa s [*Lide*, 2001]) and T_0 is the reference temperature for CO_2 ($528°$ Rankine [*Lide*, 2001]). When temperatures are expressed in Rankine $°$, the constants a and b have values of $(0.555 \, T_0) + S$ and $(0.555 \, T_{CO2}) + S$, respectively. S is Sutherland's constant, which for CO_2 has a value of $240°$ Rankine. FLOWGO conducts its calculations using Kelvin as a temperature unit. Therefore at each downflow step a temporary conversion to Rankine $°$ is required to calculate dynamic viscosity.

[60] Kinematic viscosity (ν_{atmos}) is $\eta_{atmos}/\rho_{atmos}$.

[61] Thermal conductivity (α_{atmos}) is

$$\alpha_{atmos} = A + B T_{atmos} + C T_{atmos}^2, \tag{A6}$$

A, B, and C are constants with values for CO_2 of -0.01183 W m^{-1} K^{-1}, 1.0174×10^{-4} W m^{-1} K^{-2}, and -2.2242×10^{-8} W m^{-1} K^{-3}, respectively [e.g., *Perry and Green*, 2001].

[62] Specific heat capacity (cp$_{atmos}$) is molar heat capacity divided by molecular weight. Molar heat capacity, C_{atmos}, is

$$C_{atmos} = a + b T_{atmos} + c T_{atmos}^{-2}. \tag{A7}$$

The constants a, b, and c have values of 44.2 J K^{-1} mol^{-1}, 8.8×10^{-3} J K^{-2} mol^{-1}, and -8.6×10^5 J K mol^{-1} [*Adamson*, 1979].

[63] Thermal diffusivity (β_{atmos}) is equal to T_{atmos}^{-1}.

[64] Finally, cubic expansivity (κ_{atmos}) is derived from

$$\kappa_{atmos} = g_{Mars} \, \beta_{atmos} \, \nu_{atmos}^{-2}. \tag{A8}$$

References

Adamson, A. W. (1979), *A Textbook of Physical Chemistry*, 2d ed., 953 pp., Academic, San Diego, Calif.

Baloga, S., and D. Pieri (1986), Time-dependent profiles of lava flows, *J. Geophys. Res.*, 91(B9), 9543–9552.

Bird, R. B., W. E. Stewart, and E. N. Lightfoot (1960), *Transport Phenomena*, 780 pp., John Wiley, New York.

Blanchard, D. C., and A. T. Spencer (1957), Raindrop measurements during Project Shower, *Tellus*, 9, 541–552.

Calvari, S., M. Coltelli, M. Neri, M. Pompilio, and V. Scribano (1994), The 1991–1993 Etna eruption: Chronology and lava flow-field evolution, *Acta Vulcanol.*, 4, 1–4.

Costa, A., and G. Macedonio (2003), Viscous heating in fluids with temperature-dependent viscosity: Implications for magma flows, *Nonlinear Processes Geophys.*, 10, 545–555.

Crane Company (1988), Flow of fluids through valves, fittings, and pipes, *Tech. Pap. 410*, New York.

Crisp, J. A. (1984), Rates of magma emplacement and volcanic output, *J. Volcanol. Geotherm. Res.*, 20, 177–201.

Crisp, J., and S. Baloga (1990), A model for lava flows with two thermal components, *J. Geophys. Res.*, 95(B2), 1255–1270.

Crisp, J., and S. Baloga (1994), Influence of crystallization and entrainment of cooler material on the emplacement of basaltic aa lava flows, *J. Geophys. Res.*, 99, 11,819–11,831.

Crisp, J., K. V. Cashman, J. A. Bonini, S. B. Hougen, and D. C. Pieri (1994), Crystallization history of the 1984 Mauna Loa lava flow, *J. Geophys. Res.*, 99(B4), 7177–7198.

Dragoni, M. (1989), A dynamical model of lava flows cooling by radiation, *Bull. Volcanol.*, 51, 88–95.

Fink, J. H., and J. R. Zimbelman (1986), Rheology of the 1983 Royal Gardens basalt flows, Kilauea Volcano, Hawai'i, *Bull. Volcanol.*, 48, 87–96.

Fink, J. H., and J. R. Zimbelman (1990), Longitudinal variations in rheological properties of lavas: Puu Oo basalt flows, Kilauea volcano, Hawaii, in *Lava Flows and Domes*, edited by J. H. Fink, pp. 157–173, Springer-Verlag, New York.

Flynn, L. P., and P. J. Mouginis-Mark (1994), Temperature of an active lava channel from spectral measurements, Kilauea Volcano, Hawai'i, *Bull. Volcanol.*, 56, 297–301.

Garbeil, H., S. K. Rowland, and A. J. L. Harris (2002), The effects of Martian conditions on lava flowing in a channel, *Eos Trans. AGU*, 83(47), Fall Meet. Suppl., Abstract P61D-04.

Ghiorso, M. S., and R. O. Sachs (1995), Chemical mass transfer in magmatic processes, IV. A revised and internally consistent thermodynamic model for the interpolation and extrapolation of liquid-solid equilibria in magmatic systems at elevated temperatures and pressures, *Contrib. Mineral. Petrol.*, 119, 197–212.

Greeley, R., and J. D. Iverson (1987), Measurements of wind friction speeds over lava surfaces and assessment of sediment transport, *Geophys. Res. Lett.*, 14, 145–159.

Guest, J. E., C. R. J. Kilburn, H. Pinkerton, and A. Duncan (1987), The evolution of flow fields: Observations of the 1981 and 1983 eruptions of Mount Etna, Sicily, *Bull. Volcanol.*, 49, 527–540.

Harris, A. J. L., and S. K. Rowland (2001), FLOWGO: A kinematic thermo-rheological model for lava flowing in a channel, *Bull. Volcanol.*, 63, 20–44.

Harris, A. J. L., L. P. Flynn, L. Keszthelyi, P. J. Mouginis-Mark, S. K. Rowland, and J. A. Resing (1998), Calculation of lava effusion rates from Landsat TM data, *Bull. Volcanol.*, 60, 52–71.

Harris, A. J. L., J. B. Murray, S. E. Aries, M. A. Davies, L. P. Flynn, M. J. Wooster, R. Wright, and D. A. Rothery (2000), Effusion rate trends at Etna and Krafla and their implications for eruptive mechanisms, *J. Volcanol. Geotherm. Res.*, 102, 237–270.

Harris, A. J. L., L. P. Flynn, O. Matías, and W. I. Rose (2002), The thermal stealth flows of Santiaguito dome, Guatemala: Implications for the cooling and emplacement of dacitic block-lava flows, *Geol. Soc. Am. Bull.*, 114, 533–546.

Head, J. W., and L. Wilson (1986), Volcanic processes and landforms on Venus: Theory, predictions, and observations, *J. Geophys. Res.*, 91, 9407–9446.

Hess, S. L., R. M. Henry, C. B. Leovy, J. A. Ryan, and J. E. Tillman (1977), Meteorological results from the surface of Mars: Viking 1 and 2, *J. Geophys. Res.*, 82, 4559–4574.

Hulme, G. (1974), The interpretation of lava flow morphology, *Geophys. J. R. Astron. Soc.*, 39, 361–383.

Hulme, G. (1982), A review of lava flow processes related to the formation of lunar sinuous rilles, *Geophys. Surv.*, 5, 245–279.

Jeffreys, H. (1925), The flow of water in an inclined channel of rectangular section, *Philos. Mag.*, 49, 793–807.

Johnson, A. M. (1970), *Physical Processes in Geology*, 577 pp., W. H. Freeman, New York.

Kallianpur, K., and P. J. Mouginis-Mark (2001), Slopes of Martian volcanoes, *Lunar Planet. Sci.* [CD-ROM], XXXII, Abstract 1258.

Kauahikaua, J., K. V. Cashman, T. N. Mattox, C. C. Heliker, K. A. Hon, M. T. Mangan, and C. R. Thornber (1998), Observations on basaltic lava streams in tubes from Kilauea Volcano, island of Hawai'i, *J. Geophys. Res.*, 103(B11), 27,303–27,323.

Kays, W. M., and M. E. Crawford (1980), *Convective Heat and Mass Transfer*, 420 pp., McGraw-Hill, New York.

Keszthelyi, L. (1995a), A preliminary thermal budget for lava tubes on the Earth and planets, *J. Geophys. Res.*, 100, 20,411–20,420.

Keszthelyi, L. (1995b), Measurements of the cooling at the base of pahoehoe flows, *Geophys. Res. Lett.*, 22, 2195–2198.

Keszthelyi, L., and R. Denlinger (1996), The initial cooling of pahoehoe flow lobes, *Bull. Volcanol.*, 58, 5–28.

Keszthelyi, L., and S. Self (1998), Some physical requirements for the emplacement of long basaltic lava flows, *J. Geophys. Res.*, 103(B11), 27,447–27,464.

Kieffer, H. H., T. Z. Martin, A. R. Peterfreund, B. M. Jakowsky, E. D. Miner, and F. D. Palluconi (1977), Thermal and albedo mapping of Mars during the Viking primary mission, *J. Geophys. Res.*, 82, 4249–4291.

Lide, D. R. (2001), *Handbook of Chemistry and Physics*, CRC Press, Boca Raton, Fla.

Lipman, P. W., and N. G. Banks (1987), Aa flow dynamics, Mauna Loa 1984, *U.S. Geol. Surv. Prof. Pap.*, 1350, 1527–1568.

Marsh, B. D. (1981), On the crystallinity, probability of occurrence, and rheology of lava and magma, *Contrib. Mineral. Petrol.*, 78, 85–98.

Moore, H. J. (1987), Preliminary estimates of the rheological properties of 1984 Mauna Loa lava, *U.S. Geol. Surv. Prof. Pap.*, 1350, 1569–1588.

Mordy, W. A. (1957), Geographic and climatic notes on the project shower area, *Tellus*, 9, 472–474.

Mouginis-Mark, P. J., and M. Tatsumura-Yoshioka (1998), The long lava flows of Elysium Planitia, Mars, *J. Geophys. Res.*, 103(E8), 19,389–19,400.

Oppenheimer, C. (1991), Lava flow cooling estimated from Landsat Thematic Mapper infrared data: The Lonquimay eruption (Chile, 1989), *J. Geophys. Res.*, 96, 21,865–21,878.

Perry, R. H., and D. W. Green (2001), *Perry's Chemical Engineers' Handbook*, McGraw-Hill, New York.

Pinkerton, H., and R. J. Stevenson (1992), Methods of determining the rheological properties of magmas at sub-liquidus temperature, *J. Volcanol. Geotherm. Res.*, 53, 47–66.

Pinkerton, H., and L. Wilson (1994), Factors controlling the lengths of channel-fed lava flows, *Bull. Volcanol.*, 56, 108–120.

Price, S. (1968), The unprecedented Kauai rainfall of January 1956 (abstract), in *Annotated Bibliography of Publications and Papers Relevant to Hawaiian Weather: Ninth Pacific Science Congress, 1957, Bangkok*, edited by P. C. Ekern and L. E. Worthley, *Tech. Rep. HIG-68-11*, pp. 19–20, Hawaii Inst. of Geophys., Honolulu.

Rowland, S. K. (2002), Channel development and evolution on the 1942 Mauna Loa lava flow, *Eos Trans. AGU*, 83(47), Fall Meet. Suppl., Abstract V12B-1423.

Rowland, S. K., A. J. L. Harris, and K. J. Kallianpur (2002), Vent locations on Elysium Mons, Mars, from thermal modeling of lava flows, *Lunar Planet. Sci.* [CD-ROM], XXXIII, Abstract 1441.

Rowland, S. K., H. Garbeil, and A. J. L. Harris (2004), Lava channel lengths and hazards on Mauna Loa determined from thermal and downslope modeling with FLOWGO, *Bull. Volcanol.*, in press.

Ryan, J. A., and R. M. Henry (1979), Mars atmospheric phenomena during major dust storms as measured at the surface, *J. Geophys. Res.*, 84, 2821–2829.

Ryan, J. A., R. M. Henry, S. L. Hess, C. B. Leovy, J. E. Tillman, and C. Walcek (1978), Mars meteorology: Three seasons at the surface, *Geophys. Res. Lett.*, 5, 715–718.

Sakimoto, S. E. H., and T. P. K. Gregg (2001), Channeled flow: Analytic solutions, laboratory experiments, and applications to lava flows, *J. Geophys. Res.*, 106(B5), 8629–8644.

Sakimoto, S. E. H., J. Crisp, and S. Baloga (1997), Eruption constraints on tube-fed planetary lava flows, *J. Geophys. Res.*, 102(E3), 6597–6613.

Sullivan, R., R. Greeley, M. Kraft, J. Murphy, G. Wilson, M. Golombek, K. Herkenhoff, and P. Smith (1998), Initial results for the imager for Mars Pathfinder windsock experiment, *Lunar Planet. Sci.* [CD-ROM], XXXIII, Abstract 1901.

Thordarson, T., and S. Self (1993), The Laki (Skaftar Fires) and Grimsvotn eruptions in 1783–1785, *Bull. Volcanol.*, 55, 233–263.

Wadge, G. (1981), The variation of magma discharge during basaltic eruptions, *J. Volcanol. Geotherm. Res.*, *11*, 139–168.

Wadge, G., and R. M. C. Lopes (1991), The lobes of lava flows on Earth and Olympus Mons, Mars, *Bull. Volcanol.*, *54*, 10–24.

Wilson, L., and J. W. Head (1994), Mars: Review and analysis of volcanic eruption theory and relationships to observed landforms, *Rev. Geophys.*, *32*, 221–263.

Wilson, L., and P. J. Mouginis-Mark (2001), Estimation of volcanic eruption conditions for a large flank event on Elysium Mons, Mars, *J. Geophys. Res.*, *106*(E9), 20,621–20,628.

Wooster, M. J., R. Wright, S. Blake, and D. A. Rothery (1997), Cooling mechanisms and an approximate thermal budget for the 1991–1993 Mount Etna lava flow, *Geophys. Res. Lett.*, *24*, 3277–3280.

————————————

H. Garbeil, A. J. L. Harris, and S. K. Rowland, Hawai'i Institute of Geophysics and Planetology, School of Ocean and Earth Science and Technology, University of Hawai'i at Mānoa, 2525 Correa Rd., Honolulu, HI 96822, USA. (scott@higp.hawaii.edu)